Excitation Wavelength Dependence of the Fluorescence Kinetics in Photosystem I Particles from *Synechocystis* PCC 6803 and *Synechococcus elongatus*

Bas Gobets,* Ivo H. M. van Stokkum,* Frank van Mourik,† Jan P. Dekker,* and Rienk van Grondelle*
*Division of Physics and Astronomy of the Exact Faculty of Sciences and Institute of Molecular Biological Sciences, Vrije Universiteit, Amsterdam, The Netherlands; and †Institut de Physique de la Matière Condensée, Université de Lausanne, Lausanne, Switzerland

ABSTRACT The excitation-wavelength dependence of the excited-state dynamics of monomeric and trimeric Photosystem I (PSI) particles from *Synechocystis* PCC 6803 as well as trimeric PSI particles from *Synechococcus elongatus* has been studied at room temperature using time-resolved fluorescence spectroscopy. For aselective (400 nm), carotenoid (505 nm), and bulk chlorophyll (~650 nm) excitation in all species, a downhill energy-transfer component is observed, corresponding to a lifetime of 3.4–5.5 ps. For selective red excitation (702–719 nm) in all species, a significantly faster, an ~1-ps, uphill transfer component was recorded. In *Synechococcus* PSI, an additional ~10-ps downhill energy-transfer component is found for all wavelengths of excitation, except 719 nm. Each of the species exhibits its own characteristic trap spectrum, the shape of which is independent of the wavelength of excitation. This trap spectrum decays in ~23 ps in both monomeric and trimeric *Synechocystis* PSI and in ~35 ps in trimeric *Synechococcus* PSI. The data were simulated based on the 2.5 Å structural model of PSI of *Synechococcus elongatus* using the Förster equation for energy transfer, and using the 0.6–1-ps charge-separation time and the value of 1.2–1.3 for the index of refraction that were obtained from the dynamics of a hypothetical PSI particle without red chls. The experimentally obtained lifetimes and spectra were reproduced well by assigning three of the chlorophyll-*a* (chl*a*) dimers observed in the structure to the C708/C702RT pool of red chls present in PSI from both species. Essential for the simulation of the dynamics of *Synechococcus* PSI is the assignment of the single chl*a* trimer in the structure to the C719/C708RT pool present in this species.

INTRODUCTION

Photosystem I (PSI) is one of two photosystems in oxygenic photosynthesis. It uses light energy to transfer electrons from plastocyanin or soluble cytochrome c_6 to $NADP^+$.

The PSI core is a large pigment-protein complex consisting of 11–13 protein subunits (Scheller et al., 1997, 2001), the largest two of which, PsaA and PsaB, form a heterodimer to which the majority of the core antenna pigments (chl*a* and β-carotene) as well as the reaction center (RC) co-factors are bound. In cyanobacteria the PSI core complexes can be isolated both as monomers and trimers, and both forms may exist in vivo in a dynamic equilibrium, depending on the salt (Kruip et al., 1994), the Ca^{2+} concentration, and the pH (Schwabe et al., 2001).

Trimeric PSI core particles from the cyanobacterium *Synechococcus elongatus* have been crystallized, and using x-ray diffraction the structure has been obtained at 2.5 Å resolution (Jordan et al., 2001; Fromme et al., 2001). In this structural model, 96 chl*a* molecules, 22 β-carotene molecules, two phylloquinones, and three Fe_4S_4 clusters can be distinguished at atomic resolution. Approximately one-half of the antenna chls form a roughly elliptical bowl-shaped structure around the RC, which is extended by two groups of peripheral antenna molecules. Although the RC is located in the middle of the complex, the distance of any of the antenna chls to the RC co-factors is >~18 Å, except for two chls that seem to form a ''bridge'' between the RC and the antenna. It has been suggested that these chls could play an important role in delivering excitations to the RC (Krauss et al., 1996; Schubert et al., 1997).

The PSI absorption spectrum is spectrally highly heterogeneous (see Gobets and van Grondelle, 2001). The different chl forms result from differences in the pigment-pigment and pigment-protein interactions, responsible for the shift of the absorption bands. The strongest shifts occur in the ''red'' or ''long-wavelength'' chls, which absorb at energies lower than that of the primary electron donor *P*700. It has been proposed that these red states are the result of strong pigment-pigment interactions between two or more chl molecules (Gobets et al., 1994). The number and absorption maxima of the red pools and the number of chls contained in them are highly species-dependent (Van Grondelle et al., 1994; Gobets and van Grondelle, 2001). Moreover, the red chl forms are also affected by the aggregation state of the cyanobacterial core complexes: in monomeric PSI core preparations the number of red chls is generally lower than in trimers.

On the basis of fluorescence line-narrowing (FLN) experiments (Gobets et al., 1994, 2001) it was concluded that PSI core particles from the cyanobacterium *Synechocystis* PCC 6803 at low temperatures exhibit one single inhomogeneously broadened absorption band with a maximum at 708 nm (C708) with an oscillator strength of ~3 chl*a* molecules in monomers and 4–5 chl*a* molecules in each

Submitted November 22, 2002, and accepted for publication August 22, 2003.

Address reprint requests to Rienk van Grondelle, Fax: 31-20-444-7899; E-mail: rienk@nat.vu.nl.

0006-3495/03/12/3883/16 $2.00

monomeric unit in trimers. However, on the basis of hole-burning experiments Hayes et al. (2000) concluded that in *Synechocystis* PSI trimers two different species of red chls are present, designated C706 and C714, each of which is present with an oscillator strength of two chl*a* molecules in each monomeric unit. The presence of a C714-nm pool is at odds with the fluorescence line-narrowing data, but the exact origin of the discrepancy between these two techniques remains unclear. Recently Ihalainen and co-workers presented both FLN and hole-burning data on plant PSI (Ihalainen et al., 2003). The hole-burning spectrum presented in this article was very similar to that found by Hayes and co-workers, including a 714-nm hole. Ihalainen and co-workers were, however, also confronted with the problem of consolidating these hole-burning data with the FLN data presented in the same article. Both hole-burning and FLN experiments are performed at low temperatures; room-temperature time-resolved measurements (Gobets et al., 2001) so far did not reveal the presence of more than one pool of red chls in *Synechocystis* PSI (Gobets et al., 2001), and therefore in this article we will regard the red absorption in *Synechocystis* PSI as due to a single (inhomogeneously broadened) band, C708. At room temperature this single C708 pool is blue-shifted to peak at ~702 nm (C702RT; Gobets et al., 2001; Rätsep et al., 2000). The possibility of heterogeneity in the red absorption band will be addressed.

The 4 K absorption spectrum of the trimeric core particles of the cyanobacterium *Synechococcus elongatus* clearly reveals two red chl bands with maxima at 708 nm (C708, corresponding to 4–6 chl*a* molecules) and 719 nm (C719, corresponding to ~4 chl*a* molecules; Pålsson et al., 1996). On the basis of hole-burning experiments, the presence of a third, intermediate pool of red chls with a low temperature absorption maximum at 715 nm has recently been proposed (Zazubovich et al., 2002). Such an intermediate state was not resolved in room-temperature time-resolved measurements (Gobets et al., 2001), which only indicated the presence of two spectroscopically different states responsible for the red absorption in *Synechococcus* PSI. Therefore, in this article, in dealing with room-temperature data, we will regard the red absorption in *Synechococcus* PSI as due to two different bands of red chls, C708 and C719.

Like in PSI from *Synechocystis*, the C708 pool in *Synechococcus* PSI is blue-shifted at room temperature to ~702 nm (C702RT), whereas the C719 pool is shifted to 708 nm (C708RT) (Gobets et al., 2001).

In their structural model of *Synechococcus* trimeric PSI, Jordan et al. (2001) point out three dimers and one trimer of chl*a* as putative candidates for strongly coupled red chl sites. The trimer, consisting of the chls designated as B31, B32, and B33, is located in the periphery of the antenna, whereas the dimers consisting of the chl pairs A32/B7, A38/A39, and B37/B38 are located closer to the RC. The dimer A32/B7 is located at the lumenal side of the trimerization domain, and forms hydrophobic contacts with PsaL of the adjacent monomer, and has therefore been suggested to represent the C719 pool (Jordan et al., 2001). Recently a number of alternative assignments have been proposed. The assignment by Byrdin and co-workers is similar to that of Jordan et al., except for the addition of A31 and B6 to form a tetramer A31/B6/A32/B7 responsible for the 4 K absorption at C719 nm and a putative A12/A14 dimer (Byrdin et al., 2002). Like Jordan et al. (2001), Sener and co-workers propose that the A32/B7 dimer is responsible for the C719 absorption, and they suggest two dimers, A33/A34 and A24/A35, to represent a C715 pool, as well as a dimer B22/B34, representing the C708 pool (Byrdin et al., 2002; Sener et al., 2002). They note that the trimer B31/B32/B33, although strongly coupled in the dipolar approximation, turns out to be much less strongly coupled in a full Coulombic calculation. Nevertheless, based on the environment of this trimer, as well as differences with *Synechocystis* PSI, they do not rule out that the dimer may be responsible for red absorption. Damjanovic et al. (2002), like Byrdin et al. (2002), suggest the A31/B6/A32/B7 cluster as the source of the C719 absorption, and propose the dimers B24/B25 and A26/A27 to be responsible for C715 and C708 absorption respectively (Sener et al., 2002).

The function of the red chl species is still a topic of debate. Some authors have suggested that in a nonequilibrium situation they may help to increase the efficiency of the system by concentrating excitations close to *P*700 (Mukerji and Sauer, 1990; Van Grondelle and Sundström, 1988; Van Grondelle et al., 1988; Werst et al., 1992; Holzwarth et al., 1993). Recent studies have shown, however, that the red chls actually slow down the effective rate of trapping (Gobets et al., 2001). Others argue that the red chls may have a role in photoprotection (Mukerji and Sauer, 1990; Karapetyan et al., 1999), or that they simply increase the cross section for absorption of red light by the PSI antenna (Trissl and Wilhelm, 1993), important in shadelight environments (Rivadossi et al., 1999). Although the total number of low-energy chls is small, 3–10% of the total number of chls in the PSI core antenna, they have a pronounced effect on the energy-transfer and trapping dynamics in the whole PSI system, which is evident from both time-resolved and steady-state spectroscopy experiments (for a review, see Gobets and van Grondelle, 2001).

PSI from *Synechocystis* has been the subject of many room-temperature time-resolved spectroscopy experiments (Hastings et al., 1995; Turconi et al., 1996; Savikhin et al., 1999; Savikhin et al., 2000; Melkozernov et al., 2000; Gobets et al., 2001). In all these studies one or two so-called equilibration components were observed in the dynamics. These components, which account for the energy transfer between the bulk chls and the low-energy chls, exhibited lifetimes between 2 and 6.5 ps. Trapping was consistently found to occur with a lifetime of 22–25 ps. In the few cases in which selective excitation of the low-energy chls was considered (Hastings et al., 1995; Melkozernov et al., 2000),

no significant differences between the lifetimes and (decay-associated) spectra of the downhill (bulk or aselective excitation) and uphill (red excitation) energy-transfer components was found, other than the sign of the spectrum. The room-temperature dynamics of *Synechococcus* PSI has been studied less extensively. Both Holzwarth et al. (1993) and Byrdin et al. (2000) have reported a single energy-transfer component of 7–14 ps for *Synechococcus* PSI, whereas Gobets et al. (2001) and Kennis et al. (2001) report two distinctly separate energy-transfer components with lifetimes of 3–4 and ~10 ps. All studies report a trapping lifetime of 30–38 ps in this species. So far no experiments have been reported involving selective excitation of the two pools of red chls present in this species.

Here we present a systematic time-resolved fluorescence study of monomeric and trimeric PSI from *Synechocystis*, as well as of trimeric PSI from *Synechococcus* for both aselective (see also Gobets et al., 2001) and selective excitation of the red chls. Previously we simulated the kinetics of PSI from both *Synechocystis* (Gobets et al., 1998a), and *Synechococcus* (Gobets et al., 1998b) using the 4 Å structural model (Krauss et al., 1996). A major difficulty in these simulations was that the precise orientations of the chl molecules, and in particular the directions of the transition dipole moments, were not known. The new 2.5 Å model (Jordan et al., 2001) does provide the precise chl orientations as well as the assignment of seven additional chls that could not be distinguished in the 4 Å model. We will show that our kinetic data of PSI from *Synechococcus* can, indeed, be simulated quite well using the 2.5 Å model of PSI from this species. Also the kinetics of PSI from *Synechocystis* could be reproduced quite well using the structural model of PSI from *Synechococcus*.

MATERIALS AND METHODS

The *Synechocystis* sp. PCC 6803 PSI monomers and trimers were prepared as in Kruip et al. (1993) and contain 85 ± 10 chl*a*/*P*700. The trimeric PSI complexes from the thermophilic cyanobacterium *Synechococcus elongatus* were isolated as in Fromme and Witt (1998) and contain ~100 chl*a*/*P*700.

For the fluorescence experiments the samples were diluted to an OD_{680} of 0.6/cm with a buffer containing 20 mM $CaCl_2$, 20 mM $MgCl_2$, 10 mM 2-(*n*-morpholino)ethane sulfonic acid, and 0.05% W/V dodecyl-β-D-maltoside at a pH of 6.5. 10 mM Sodium ascorbate and 10 μM phenazine meta sulfate were added to all samples to prevent accumulation of $P700^+$. To avoid multiple excitation of the same sample volume by successive laser flashes the sample was contained in a spinning cell (diameter, 10 cm) rotating at 20 Hz. All experiments were performed at room-temperature (293 K). The experimental setup and procedures as well as the data processing were described in detail in Gobets et al. (2001). In short, the samples were excited using 150–200-fs pulses at 400, 505, 650/660, 702, 710, and 719 nm, which were generated at a 100-kHz repetition rate using a Titanium:sapphire based oscillator (Mira, Coherent, Santa Clara, CA), a regenerative amplifier (Coherent REGA), and a double-pass optical parametric amplifier (Coherent OPA-9400).

The excitation light was focused with a 15-cm focal length lens, resulting in a focal diameter of 150 μm in the sample. Fluorescence was collected at right angle to the excitation using achromatic lenses and detected through a sheet polarizer set at magic angle (54.7°), or perpendicular to the polarization of the excitation light, using a Hamamatsu (Hamamatsu City, Japan) C5680 synchroscan streak camera and a Chromex (Albuquerque, NM) 250IS spectrograph. The streak-images were recorded on a Hamamatsu C4880 charge-coupled device camera which was cooled to −55°C. The full-width at half-maximum of the overall time-response of this system is 3–3.5 ps. The spectral resolution was 8 nm. One streak image covers 315 nm in the spectral domain (1018 pixels) and 200 ps (1000 pixels) in the time-domain. The applied pulse energy was varied between 1 and 4 nJ, depending on the wavelength of excitation, such that typically only 0.25% of all chls present in the focus was excited by each pulse, thus avoiding singlet-singlet annihilation.

In the data analysis a Gaussian-shaped instrument response function was assumed. The width of this Gaussian was a free parameter of the fit (typically 3–3.5 ps). In some cases the fit was improved by allowing for a small additional contribution (~5%) of a broader Gaussian to the instrument response.

All measurements were analyzed using a model with a number of parallel compartments, which yields decay-associated spectra (DAS). Some restrictions were imposed on the instantaneous spectrum (see Table 1). For measurements in which a (Raman) scattering contribution was present, a pulse-limited contribution was included in the fit, in addition to the exponentially decaying components. In some of these measurements, a small (5–10%) pulse-limited contribution was present at a time later than time *zero*. This contribution, which was assigned to a reflection, was fitted by allowing for a second pulse in the analysis, which exhibited the same width as the instrument response, but which was delayed by a certain time.

The periodicity of the synchroscan with a period of 13.4 ns results in a back-and-forth sweeping of long-lived (>1-ns) components, evident from

TABLE 1 Restrictions used in global analysis

		(Raman) scatter zero		Time *zero* spectrum zero	
Sample	λ_{ex} (nm)	Below (nm)	Above (nm)	Below (nm)	Above (nm)
Synechocystis monomers	400	–	–	–	665
	505	–	640	–	665
	660	–	670	660	695
	702	688	713	688	–
	710	685	730	685	–
Synechocystis trimers	400	–	–	–	665
	702	688	713	688	–
	710	685	730	685	–
Synechococcus trimers	400	–	–	–	665
	650	–	–	–	–
	710	690	725	675	–
	719	710	730	690	–

the signal present before time *zero* (the time of the maximum of the instrument response function). By taking this into account in the analysis, the lifetime and spectrum of a (single) long-lived component (such as some free chl present in the sample) could be estimated accurately on the 200-ps timescale.

RESULTS

Room-temperature absorption spectra

Fig. 1 displays the room-temperature absorption spectra of the three PSI preparations that were studied. Clearly the spectra are quite similar; the only significant differences occur in the red edge of the Q_y absorption band, at wavelengths longer than ~700 nm, reflecting the variation in the amounts and energies of red-shifted chlorophylls (chls) between the three species.

Monomeric PSI from *Synechocystis* (*solid*) exhibits the least amount of these red chls. The trimeric PSI from the same species (*dotted*) shows slightly more red chl absorption, while trimeric PSI from *Synechococcus* (*dashed*) clearly contains considerably more red chls than the other two preparations. These observations are consistent with other room- and low-temperature estimates of the numbers of red chls contained in these PSI particles (Gobets et al., 2001).

Fig. 1 also indicates the wavelengths of excitation used in the time-resolved fluorescence measurements. At 400 nm mainly the Soret-band of chl*a* is excited, and excitation is considered to be aselective at this wavelength. With 505-nm light the β-carotene molecules are predominantly excited. These molecules are known to transfer energy efficiently to chl*a* (Kennis et al., 2001; Van der Lee et al., 1993). The blue edge of the bulk Q_y absorption band is excited at 650/660 nm. At 702 nm the excitation is relatively selective both for *P*700 and the C708/C702RT pool of red chls. More selective excitation of the red-most chl pools is achieved at 710 nm and 719 nm.

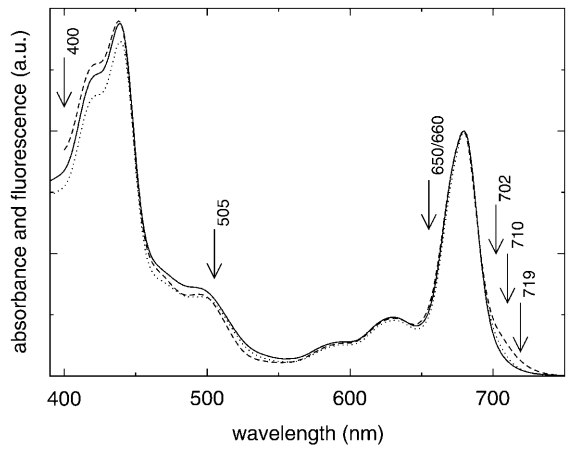

FIGURE 1 Room-temperature absorption spectra of monomeric (*solid*) and trimeric (*dotted*) PSI from *Synechocystis* PCC6803 and trimeric PSI from *Synechococcus elongatus* (*dashed*). Note the clear differences in red chl content. Arrows indicate the wavelengths of excitation that were used in the experiments. The spectra were normalized to the maximum in the Q_y region.

For some excitation wavelengths, scattered excitation light was recorded along with the fluorescence. In these experiments the polarization of the detection was chosen perpendicular to the polarization of the exciting laser light, to reduce the amount of scattering. In principle this could result in anisotropic lifetime components in the measurements. However, since the major fraction of depolarization is fast (~150 fs; Kennis et al., 2001; Du et al., 1993), and most of the observed lifetime components are not related to a single transfer step between two specific chromophores, but rather to an ensemble average of many different transfer steps between many differently oriented chls, the polarization effects will, to a large extent, average out for these components. We will discuss the possibility of polarization effects for the fastest components. For the wavelengths of excitation that were outside the fluorescence detection range (i.e., 400 nm and 505 nm), the polarization of the detection was at magic angle (54.7°) to the polarization of the excitation light.

Time-resolved fluorescence measurements

Figs. 2–4 show the decay-associated spectra that result from the global analysis of the time-resolved fluorescence data for the three PSI preparations for the different wavelengths of excitation. For details on the interpretation of DAS for a system such as PSI we refer to Gobets and van Grondelle (2001). Data for 400-nm excitation have been reported before, but have now been analyzed requiring the absence of instantaneous fluorescence in the Q_y region (Gobets et al., 2001). Fast rise components in the Q_y region are also found in the analysis without this explicit restriction, but the DAS improve significantly upon applying these constraints. For other wavelengths of excitation similar restrictions were imposed in the analysis, which are listed in Table 1. In the cases for which a significant difference occurs between the shown, restricted analysis and the fit without restrictions (not shown), this will be addressed. The pulse-limited (Raman) scatter contributions were also restricted to the wavelength range in which they are expected (Table 1). All the lifetimes of the global analysis of the three preparations for all wavelengths of excitation used are listed in Table 2.

Synechocystis PSI monomers

The 400-nm light preferentially excites the Soret band of chl*a*, which relaxes to the lowest excited singlet (Q_y) state in a few hundred fs. The Soret-Q_y ingrowth is reflected by a component which is represented by a DAS (Fig. 2 *a*, *solid*) which is negative throughout the whole Q_y region with a minimum at 688 nm, and which is fitted with a lifetime of 0.8 ps. The second component exhibits a lifetime of 5.5 ps

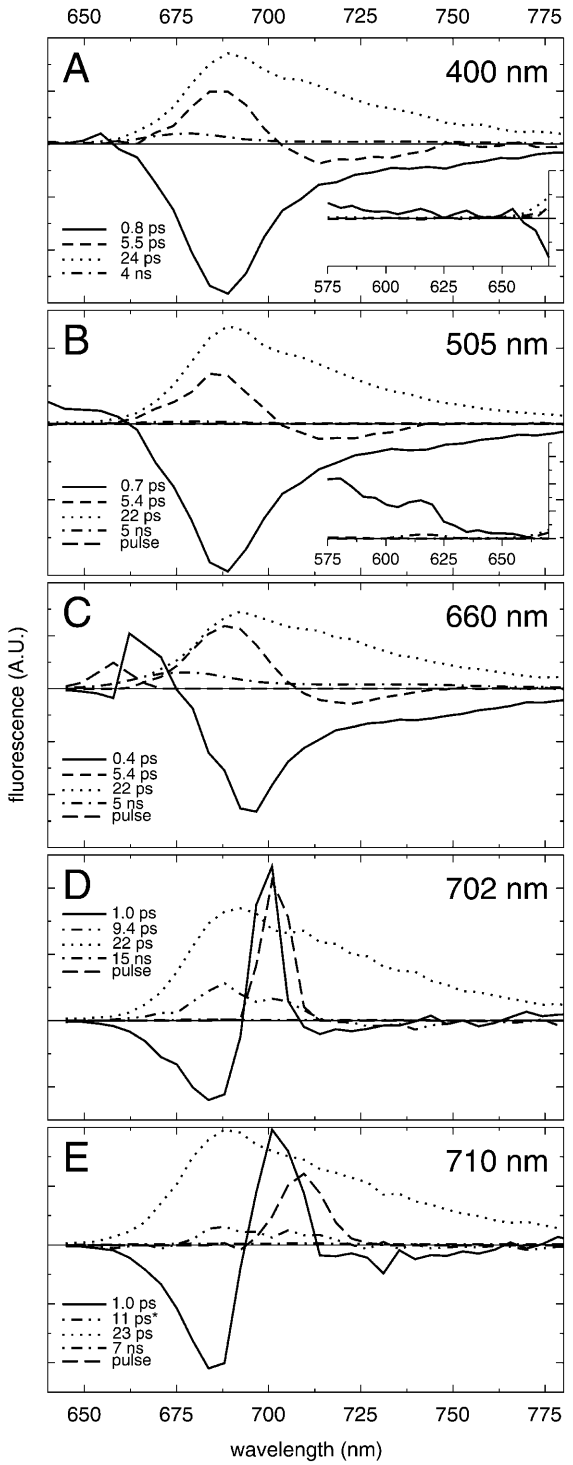

FIGURE 2 Decay-associated spectra of fluorescence decay of monomeric PSI from *Synechocystis* PCC6803 for excitation at 400 nm (*A*), 505 nm (*B*), 660 nm (*C*), 702 nm (*D*), and 710 nm (*E*). Note that the scaling of the *y* axis of each of the insets corresponds to that of the main graph.

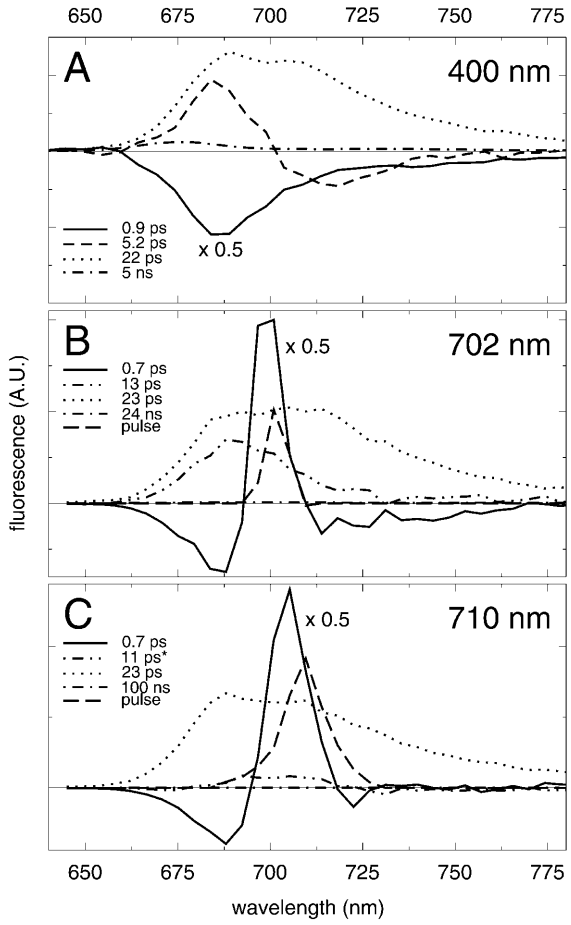

FIGURE 3 Decay-associated spectra of fluorescence decay of trimeric PSI from *Synechocystis* PCC6803 for excitation at 400 nm (*A*), 702 nm (*B*), and 710 nm (*C*).

and is represented by a DAS (*dashed*) which is positive in the blue part of the spectrum, peaks at ~687 nm, and drops below zero at wavelengths longer than 703 nm. (In an analysis without restrictions, this equilibration component was fitted with a somewhat shorter lifetime of 4.4 ps; Gobets et al., 2001.) Such a DAS, which represents a decay of fluorescence in one part of the spectrum and a rise of fluorescence in another part, is indicative of energy transfer between spectrally different chromophores. This component therefore reflects energy transfer from bulk chls emitting at ~687 nm, to red-shifted chls emitting at ~712 nm (Gobets et al., 2001), thus creating a thermally (more) equilibrated distribution of excitations. However, the DAS is not conservative, i.e., the positive area is somewhat larger than the negative area, indicating that effectively some excitations disappear during this process. For a ''pure'' transfer component, no loss of excitations would occur; therefore, we conclude that this component also includes some non-equilibrium trapping (i.e., trapping occurring before all equilibration processes are completed; Gobets et al., 2001). The third component is fitted with a lifetime of 24 ps, and an all-positive DAS (*dotted*) that peaks at ~690 nm and exhibits a broad shoulder at ~712 nm. This component represents the decay of excitations from a more or less

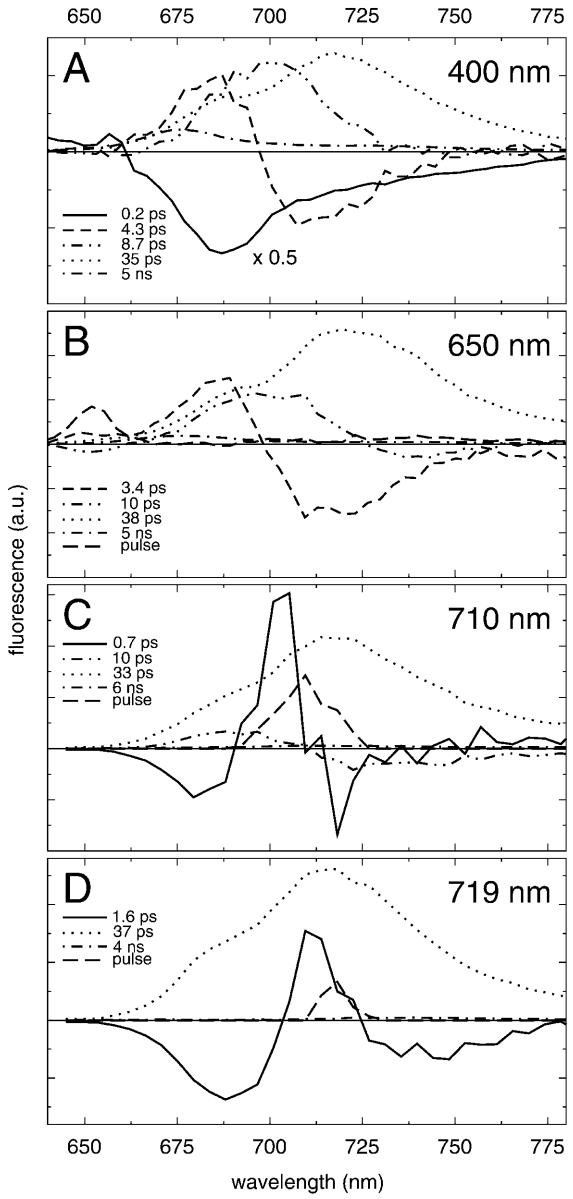

FIGURE 4 Decay-associated spectra of fluorescence decay of trimeric PSI from *Synechococcus elongatus* for excitation at 400 nm (*A*), 650 nm (*B*), 710 nm (*C*), and 719 nm (*D*).

thermally equilibrated distribution of excitations, due to trapping of the excited state energy by charge-separation in the RC. This component will therefore be referred to as the trap component.

The slowest component, representing a small fraction of uncoupled chls in the preparation, is fitted with a 4-ns lifetime, and a DAS (*dot-dashed*) which peaks at 678 nm and has a shape which is typical for chl*a* in solution.

The inset shows the DAS in the 575–675 nm region, which are all zero, except for the fastest (0.8-ps) component. The small positive amplitude of this component may indicate some carotenoid excitation at 400 nm (see below).

Excitation at 505 nm (Fig. 2 *b*) preferentially excites β-carotene, which efficiently transfers excitations to chl*a* (Kennis et al., 2001; Van der Lee et al., 1993). The results are almost identical to those for 400-nm excitation, although at this excitation wavelength the sub-ps ingrowth in the Q_y region (*solid*) is accompanied by a large positive contribution in the region <660 nm (see *inset*), indicating that this component represents energy transfer from β-carotene to chl*a* rather than Soret to bulk equilibration. Raman scattering of the excitation light by water (at 3600 cm^{-1} from the excitation wavelength) results in a pulse-limited contribution (*long-dashed*) ~615 nm. The amplitude of the component representing uncoupled chls (*dot-dashed*) is significantly reduced with respect to 400-nm excitation, due to the low absorption of chl*a* at 505 nm.

The main results for 660-nm excitation (Fig. 2 *c*) are almost identical to those for 400-nm and 505-nm excitation. The difference in excitation wavelength is mainly expressed by the fastest lifetime component (0.4 ps, *solid*), which shows a decay at ~665 nm, and therefore represents energy transfer (equilibration) within the Q_y absorption band (Kennis et al., 2001; Du et al., 1993). This energy-transfer spectrum is nonconservative (the area of the positive part of the spectrum is smaller than that of the negative part), which may to a large extent be attributed to depolarization, since only the perpendicular fraction of the fluorescence was recorded for this wavelength of excitation (see above).

The 5.4-ps component (*dashed*), representing energy transfer between the bulk and red chls, exhibits a spectrum that shows a significantly larger amplitude in the positive region, which may reflect that the amount of nonequilibrium trapping is larger for 660-nm excitation, as compared to excitation at 400 nm and 505 nm. A pulse-limited contribution (*long-dashed*) accounts for the scatter contribution present around the excitation wavelength.

The results for 702-nm excitation (Fig. 2 *d*), selective for both *P*700 and the red chls of the C708/C702RT pool, differ substantially from the results for the three excitation wavelengths discussed so far. The fastest process (*solid*), is fitted with a 1-ps lifetime and a spectrum which is negative at ~685 nm, positive at ~700 nm, and again slightly negative in the red part of the spectrum. This component reflects the uphill energy-transfer from the initially excited red-shifted chl forms to the bulk antenna chls. The lifetime of this uphill energy-transfer is remarkably short compared to the ~5.5-ps downhill energy-transfer lifetime observed for the previously discussed wavelengths of excitation and, apart from the sign, the shape of the uphill transfer spectrum also differs significantly from the downhill spectra. These differences cannot be explained in terms of simple compartmental models (Gobets et al., 2001). The results for 702-nm excitation also feature a process characterized by a 9.4-ps lifetime and an all-positive spectrum (*double-dot-dashed*) exhibiting a double-banded structure with maxima at 688 nm and 702 nm. The origin of this component is not clear. It

TABLE 2 Lifetimes observed in PSI of *Synechocystis* and *Synechococcus*

	Energy-transfer components (ps)				Trapping (ps)		
λ_{ex} (nm)	Soret and Car to Q_y	Within bulk Q_y	Bulk to red	Red to bulk	Fast	Normal	Long-lived (ns)
Synechocystis monomers							
400	0.8	–	5.5	–	–	24	4
500	0.7	–	5.4	–	–	22	5
650	–	0.4	5.4	–	–	22	5
700	–	–	–	1.0	9.4	22	15†
710	–	–	–	1.0	11*	23	7†
Synechocystis trimers							
400	0.9	–	5.2	–	–	22	5
700	–	–	–	0.7	13	23	24†
710	–	–	–	0.7	11*	23	100†
Synechococcus trimers							
400	0.2	–	4.3 and 8.7	–	–	35	5
650	–	–	3.4 and 10	–	–	38	5
710	–	–	10	0.7	–	33	6†
719	–	–	–	1.6	–	37	4†

*Fixed value.
†Minor amplitudes.

does not arise in compartmental (Gobets et al., 2001) nor structure-based modeling (Gobets et al., 1998a, and see below). Since the spectrum is positive at all wavelengths, it seems to be a fast trapping component. However, for this wavelength of excitation, a ''normal'' trapping component is also recorded (*dotted*), with a lifetime and spectrum identical to those found for the other wavelengths of excitation. The fit also includes a component with a lifetime of 15 ns, with an almost negligible amplitude (*dot-dashed*) and a pulse-limited contribution (*long-dashed*) to account for the scattered excitation light.

Excitation with 710-nm light leads to an almost exclusive excitation of the red chls. The results for this wavelength of excitation (Fig. 2 *e*) are similar to those for 702-nm excitation. Uphill energy-transfer occurs in 1 ps. The corresponding spectrum (*solid*) has more or less the same shape as for 702-nm excitation, but has a larger amplitude: the more red-shifted excitation wavelength leads to a larger nonequilibrium initial distribution of excitations, resulting in a larger amplitude of the equilibration component. The remarkable 9.4-ps component that appeared in the analysis for 702-nm excitation does not appear directly in the analysis for 710-nm excitation. However, it was found that the introduction of a component with a fixed 11-ps lifetime resulted in an improved fit, and a spectrum similar to the 9.4-ps component found for 702-nm excitation, albeit with a smaller amplitude (Fig. 2 *e*, *double-dot-dashed*). Since no ~10-ps component could be found for the other wavelengths of excitation, it seems that the ~10-ps process is somehow related to the direct excitation of chls absorbing at ~700 nm.

Also, for this wavelength of excitation, the trapping component (23 ps, *dotted*) appears identical to that for the other wavelengths of excitation. The scattered excitation light at 710 nm was accounted for by a pulse-limited contribution (*long-dashed*).

Synechocystis PSI trimers

The results for the PSI trimers of *Synechocystis* for excitation at 400, 702, and 710 nm are displayed in Fig. 3. All the lifetimes and spectra are similar to those observed for the monomers for the corresponding wavelengths of excitation. However, the amplitude of both the uphill (Fig. 3 *a*, *dashed*) and downhill (Fig. 3, *b* and *c*, *solid*) energy-transfer spectra appear to be somewhat larger in trimers than in monomers, and also the trapping spectra (Fig. 3, *a–c*, *dotted*) display a more pronounced shoulder at ~710 nm in the trimers. Both these observations are attributed to the larger number of red chls contained in the trimers as compared to the monomers. Also for trimers, the analysis for 702-nm excitation yields an ~10-ps component with an all-positive spectrum (Fig. 3 *b*, *double-dot-dashed*, 13 ps), ruling out the possibility that this component is a monomerization artifact. For 710-nm excitation, as for monomers, the introduction of a fixed 11-ps component lead to an improved fit, and an all-positive spectrum with a small amplitude (Fig. 3 *b*, *double-dot-dashed*).

Synechococcus PSI trimers

PSI trimers from *Synechococcus elongatus* contain a significantly larger number of red chls as compared to PSI from *Synechocystis*. Moreover, they appear in two distinct pools, one of which is significantly lower in energy as compared to the PSI particles from *Synechocystis*. Consequently, the energy-transfer and trapping dynamics in *Synechococcus* PSI differ substantially from those of PSI from *Synechocystis* (Fig. 4).

In Fig. 4 *a*, the results are shown for excitation of the chl*a* Soret transition at 400 nm. The fastest component is fitted with a 0.2-ps lifetime, and expresses the Soret to Q_y

relaxation (*solid*). As for *Synechocystis* PSI, this ingrowth shows a distinct minimum ~687 nm, yet it features a much more pronounced wing above ~700 nm, reflecting the larger number and lower energies of the red chls contained in this species. A process with a 4.3-ps lifetime features an energy-transfer spectrum (*dashed*) that displays a significantly deeper and more pronounced minimum in the negative region of the spectrum than the ~5.5-ps downhill energy-transfer spectra of *Synechocystis* PSI. Therefore, in contrast to *Synechocystis* PSI, the total spectrum is basically conservative. The minimum of this spectrum appears at about the same wavelength as in *Synechocystis* PSI, which indicates that this component mainly accounts for equilibration of the bulk chls with the C708/C702RT pool of red chls present in both species.

A third component, with a lifetime of 8.7 ps, exhibits a spectrum (*double-dot-dashed*) which peaks at ~700 nm, and drops only slightly below zero at wavelengths longer than 730 nm. We assign this component to equilibration between the equilibrated bulk and C708/C702RT pools on the one hand and C719/C708RT red chl pool on the other hand, together with a significant amount of nonequilibrium trapping (see also Gobets et al., 2001).

A fourth component, with a 35-ps lifetime, exhibits a spectrum which is positive at all wavelengths and reflects the trapping from the equilibrated distribution of excitations. The maximum of this spectrum (*dotted*) appears at ~719 nm, reflecting that due to the larger number, and lower energies of the red chls in *Synechococcus* PSI, the equilibrium distribution is red-shifted considerably with respect to *Synechocystis* PSI. The contribution of the bulk chls is reduced to just a shoulder at ~690 nm. A small fraction of uncoupled chls present in the preparation is represented by a small 5-ns contribution (*dot-dashed*).

The results for 650-nm excitation, presented in Fig. 4 *b*, are similar to those for 400-nm excitation. The 3.4-ps and 10-ps equilibration components (*dashed* and *double-dot-dashed*) correspond to the 4.3-ps and 8.7-ps components for 400-nm excitation. The 10-ps component more clearly reveals its energy-transfer character; it is, beyond doubt, negative above ~725 nm. The 38-ps trapping component (*dotted*) is identical to that for 400-nm excitation, and some uncoupled chls are evident from a small 5-ns component (*dot-dashed*). The scattered excitation pulse is accounted for by a pulse-limited contribution (*long-dashed*) peaking at 650 nm.

With 710-nm excitation light, both pools of red chls are selectively excited (Fig. 4 *c*). The results for this wavelength of excitation differ significantly from those for 400-nm and 650-nm excitation. The fastest equilibration component is fitted with a 0.7-ps lifetime and a spectrum (*solid*) resembling that for the ~1-ps components found for 702-nm and 710-nm excitation of *Synechocystis* PSI. Since the negative part to the red side of the excitation light is only small, it seems that this fast energy-transfer component mainly involves equilibration of the first pool of red chls with the bulk chls, like the 3–4-ps components found for 400-nm and 650-nm excitation. A second equilibration component, fitted with a 10-ps lifetime (*double-dot-dashed*), bears resemblance to the ~10-ps component observed for 400-nm and 650-nm excitation. The amplitude of the spectrum is smaller, however, and the zero crossing seems to be significantly blue-shifted. The spectrum also seems much more conservative. Nevertheless we assign this component to the same processes as the ~10-ps component observed for 400-nm and 650-nm excitation. The trapping component, fitted with a 33-ps lifetime (*dotted*), is identical to that of the other wavelengths of excitation. Also at this wavelength of excitation a small 6-ns component was present. The scattered excitation light is accounted for by a pulse-limited contribution (*long-dashed*).

Excitation at 719 nm is mostly selective for the C719/C708RT pool of red chls. For this wavelength of excitation only one equilibration component can be distinguished. This component is fitted with a 1.6-ps lifetime and a spectrum (*solid*) which exhibits a positive contribution at ~712 nm and negative contributions at ~690 nm and at wavelengths longer than 725 nm. This component therefore represents both uphill and downhill energy-transfer, effectively resulting in a broadening of the initially excited distribution to the equilibrated distribution. Trapping from the equilibrated distribution (*dotted*) occurs in 37 ps, and the equilibrated spectrum (*dotted*) is identical to the trapping DAS found at other wavelengths of excitation. Also for this wavelength of excitation a small 4-ns component was found (*dot-dashed*). The scattered excitation light is accounted for by a pulse-limited contribution (*long-dashed*).

Summary of results

Synechocystis PSI contains a single pool of red chls with an absorption maximum at 702 nm at room temperature (C702RT). For all wavelengths of excitation *Synechocystis* PSI (both monomers and trimers) exhibits a single equilibration component, which is directed downhill for aselective excitation (400, 505, and 660 nm) and uphill for selective excitation in the red chl region (702 and 710 nm). The uphill transfer components are distinctly different from the downhill transfer components, both in lifetimes (0.7–1 ps uphill vs. ~5.5 ps downhill) and in spectral shape.

From the analysis for excitation at 702 nm and 710 nm a ~10-ps component emerges that exhibits an all-positive (double-banded) spectrum. The nature of this component remains unclear, but it seems to be related to excitation of chls absorbing at ~700 nm.

For all wavelengths of excitation *Synechocystis* PSI exhibits a trapping component that decays in ~23 ps. The spectrum of this component exhibits a maximum at ~690 nm and a shoulder at ~710 nm, which is more pronounced in

trimers than in monomers, due to the larger red chl content of the trimers.

In contrast to PSI from *Synechocystis*, PSI from *Synechococcus* exhibits two distinct pools of red chls with room-temperature absorption maxima at 702 and 708 nm (C702RT and C708RT). Consequently, for 400-nm, 650-nm, and 719-nm excitation, two separate energy-transfer components were distinguished in *Synechococcus* PSI, with distinctly different lifetimes. The fastest of these two components in all cases seems to reflect the equilibration between the bulk chls and the C702RT pool, whereas the slower component is associated with both nonequilibrium trapping and the equilibration between, on the one hand, the equilibrated distribution on the bulk chls and the C702RT pool, and, on the other hand, the C708RT pool.

For relatively aselective excitation (400 and 650 nm) the fastest equilibration component is directed downhill, and exhibits a lifetime of 3–4 ps, and a spectrum that resembles the downhill equilibration spectra found for *Synechocystis* PSI, albeit more conservative. For excitation at 710 nm, the fastest equilibration component is directed (mainly) uphill, and is fitted with a much shorter lifetime of 0.7 ps, similar to *Synechocystis* PSI. For all three wavelengths of excitation the slow energy-transfer is directed downhill with a lifetime of ~10 ps. The amplitude of this component is significantly lower for 710-nm excitation than for aselective excitation.

The data for 719-nm excitation reveals only one single equilibration component, reflecting both up and downhill transfer with a lifetime of 1.6 ps.

For all wavelengths of excitation, an identical trapping component was resolved with a lifetime of ~35 ps and a spectrum that exhibits a broad band with a maximum at ~719 nm, and a shoulder at ~690 nm.

In the next section we will numerically simulate most of these results.

SIMULATIONS

To understand the processes that were summarized above and the timescales on which they occur, we performed a simulation of the kinetic data based upon the recent 2.5 Å structural model of trimeric PSI from *Synechococcus elongatus* (Jordan et al., 2001). Although the dipole-dipole approximation may not hold for all pairs of chls in the PSI, and in some cases the interaction strength between chls may be considerable, we chose, for a simulation, one based on Förster energy-transfer.

Procedure

We calculated the transfer rates between the 96 different chls in the system using the Förster equation (Förster, 1965; Kleima et al., 2000; Van Amerongen et al., 2000),

$$k_{DA} = \frac{k_r^D}{n^4} \times \frac{\kappa_{DA}^2}{R_{DA}^6} \times I_{DA}, \quad (1)$$

in which k_{DA} is the rate of transfer of an excitation from a donor chl (D) to an acceptor chl (A) in ps^{-1} and k_r^D is the radiative lifetime of chl*a*, for which we use the value $5.4 \times 10^{-5}\ ps^{-1}$ (Kleima et al., 2000). n is the index of refraction of the protein. R_{DA} is the distance between donor and acceptor in nm. R_{DA} was determined by taking the distance between the centers of the four coordinating nitrogen atoms N_A–N_D for each pair of chls in the structure. κ is an orientational factor defined by

$$\kappa = (\hat{\mu}_A \times \hat{\mu}_D) - 3(\hat{\mu}_A \times \hat{r}_{AD})(\hat{\mu}_D \times \hat{r}_{AD}), \quad (2)$$

in which $\hat{\mu}_A$ and $\hat{\mu}_D$ represent the normalized Q_y transition dipole moment vectors and $\hat{r}_{AD}$ represents the vector connecting the centers of both transition dipole moments, normalized to unity. For each chl*a* molecule in the structure the vector connecting the nitrogen atoms N_B and N_D was taken to represent the direction of the Q_y transition dipole moment vectors. $\hat{r}_{AD}$ was calculated as the normalized vector connecting the centers of the four coordinating nitrogen atoms N_A–N_D for each pair of chls in the structure.

The factor I_{DA} in Eq. 1 represents the overlap integral between the donor chl emission spectrum and the acceptor chl absorption spectrum defined by Kleima et al. (2000) as

$$I_{DA} = 8.8 \times 10^{17} \times \int \frac{\varepsilon_A(n) \times F_D(\nu)}{\nu^4} d\nu, \quad (3)$$

where $\varepsilon_A(\nu)$ represents the acceptor absorption spectrum scaled to the value of the extinction coefficient (in $M^{-1}\ cm^{-1}$) in the absorption maximum and $F_D(\nu)$ represents the emission spectrum of the donor, normalized to unit area. Both spectra are on a frequency scale (cm^{-1}). The overlap integral I_{DA} was calculated for five spectrally different chl pools: a bulk chl pool with an absorption maximum at 680 nm; a pool at 686 nm representing the two chls at the A_0 (Kumazaki et al., 1994; Gobets and van Grondelle, 2001) position; a pool representing $P700$ peaking at 698 nm; and two red chl pools with room-temperature absorption maxima at 702 and 708 nm (Gobets and van Grondelle, 2001; Gobets et al., 2001). The spectra that were used to calculate the overlap integrals are listed in Table 3. The overlap integrals were calculated using Eq. 3 for downhill energy-transfer only, i.e., for pairs DA in which the absorption of D peaks at higher or equal energy as compared to the absorption of A. The complementary, downhill rates had to comply with the concept of detailed balance and were thus calculated as $k_{ij} = k_{ji} \times e^{-(E_j - E_i)/k_B T}$. We used $7.7 \times 10^4\ M^{-1}\ cm^{-1}$ as the value of the maximum of the extinction coefficient of the bulk pools, which is the value reported by Lichtenthaler for chl*a* in 80% acetone (Lichtenthaler, 1987). The absorption spectra of the other pools were scaled to those of the bulk pool by requiring them to have equal areas.

TABLE 3 Absorption and emission spectra used for overlap integrals

Pool	Absorption spectrum	Absorption max (nm)	Emission spectrum	Emission max (nm)
Bulk C680	chl*a* in acetone	680[†]	chl*a* in acetone	687[†]
A_0, C686		686[†‡]		693[†]
*P*700	Gaussian, 19 nm FWHM	698[‡]	C702 emission[‡]	708[†]
Red pool C702RT*	Gaussian, 12 nm FWHM	702	C702 emission[‡]	712
Red pool C708RT*	Gaussian, 19 nm FWHM	708	C708 emission[‡]	722

FWHM is full-width at half-maximum.
*The red pools C702 and C708 represent the respective room-temperature equivalents of the C708 and C719 red pools found at low temperatures in cyanobacterial PSI (Gobets et al., 2001).
[†]Shifted to this wavelength.
[‡]See Gobets and van Grondelle (2001).

Using the same procedure as outlined above, we have performed a simulation of the dynamics of a PSI particle not containing any red chls (Gobets et al., unpublished data). Previously it was found that such a PSI particle should exhibit a 18-ps trapping time (Gobets et al., 2001). This condition could only be met for certain combinations of the index of refraction, n (corresponding to a certain value of the average single site lifetime τ_{ss}), and the rate of charge-separation from each of the two chls constituting *P*700, γ. Consistent with the experimental results reported in Kennis et al. (2001) and Du et al. (1993), we use a value for τ_{ss} of 150 fs, corresponding to a value of γ of 1 ps^{-1}. This choice of parameters yields a value of $n = 1.2$ (for a value of the extinction-coefficient of $7.7 \times 10^4\ M^{-1}\ cm^{-1}$ and a radiative rate of $5.4 \times 10^{-5}\ ps^{-1}$; Gobets et al., unpublished data). This leaves us with no free parameters, except for the spectral composition of the antenna, which we construct by assigning each of the 96 chls to one of the five pools. In the simulations we assigned *P*700 and A_0 to their respective pools, and all the chls that were not assigned to one of the red chl pools were assigned to the bulk pool. Differences between the (simulated) dynamics of different PSI particles therefore arise solely from the differences in red chl assignments. Once the red chls have been assigned we can calculate all 96×96 pairwise energy-transfer rate constants using Eq. 1. These energy-transfer rate constants and γ are subsequently used to construct the 96 coupled linear differential equations describing the dynamics of the system. Solving these equations one obtains the 96 different eigenvalues (lifetimes) of the system. By subsequently choosing the distribution of excitations at time *zero* (i.e., aselective excitation, preferential excitation of a red pool) one imposes boundary conditions to the system which enable the calculation of the DAS corresponding to each of these lifetimes.

Because we only consider processes occurring in the Q_y region, and since we do not include heterogeneity in the bulk, the sub-ps processes of Soret-Q_y relaxation as well as bulk equilibration are not considered in the simulation.

Simulation of the dynamics in *Synechococcus* PSI

In the framework of the structure-based simulation, outlined above, we only have to assign the red chls in the structure to calculate the dynamics of the *Synechococcus* PSI. Jordan et al. (2001) point out three dimers and one trimer of chl*a* in their structural model for PSI of *Synechococcus* as being putative candidates for strongly coupled red chl sites. The trimer, consisting of the chls designated as B31, B32, and B33, is located in the periphery of the antenna, whereas the dimers consisting of the chl pairs A32/B7, A38/A39, and B37/B38 are located closer to the RC. The dimer A32/B7 is located at the lumenal side of the trimerization domain, and forms hydrophobic contacts with PsaL of the adjacent monomer, and has therefore been suggested to represent part of the C719 pool, since the amplitude of this pool depends on the aggregation form of the complex (Pålsson et al., 1998). An important parameter determining the coupling strength between a pair of chls is the distance, R, that separates them. However, the relative orientation is also an important parameter. We have, therefore, for each pair of chls considered the value of κ^2/R^6 (see Eq. 1) as a measure of the dipolar coupling strength; of course pigment-protein interactions also play an important role, as well as higher-order Coulombic terms. The κ^2/R^6 criterion yields *P*700 as being, by far, the most strongly coupled dimer in the complex. The two pairwise couplings in the trimer are the second and third strongest couplings according to this criterion. This suggests that the trimer constitutes the C719/C708RT pool rather than the A32/B7 dimer proposed by Jordan's group. Moreover, we were not able to obtain an acceptable simulation of the data with the A32/B7 dimer included in the C719/C708RT pool (see below). Interestingly, this is at odds with the idea that the C719/C708RT pool should be located within the trimerization domain. We also note that, according to the κ^2/R^6 criterion, there are three more dimers in the periphery of the structure that are at least as strongly coupled as the dimers proposed by Jordan et al. (2001), i.e., chl pairs A12/A14, A10/A18, and B09/B17. We do note that recently other assignments have been proposed (Byrdin et al., 2002, 2000; Sener et al., 2002; Damjanovic

et al., 2002; see Introduction and below). However, for now we will perform the simulation using the trimer and dimers indicated by Jordan et al. (2001) with the trimer representing the C719/C708RT pool and the three dimers representing the C708/C702RT pool. We considered three different excitation conditions: aselective (corresponding to 400-nm excitation, and more or less to 650 nm; all chls have equal probability to be excited at time *zero*), 710-nm excitation (corresponding to the excitation of a mixture of the *P*700, C708/C702RT, and C719/C708RT pools in a 1:1:1 probability ratio of excitation of the chls in each of these pools), and 719-nm excitation (corresponding to a 1:1:2 probability ratio of excitation of the chls in each of these pools). The 96 lifetimes resolved in the simulation each correspond to a separate DAS. However, if no significant increase or decay of the excitation density in any of the pools occurs with a particular lifetime, the corresponding DAS will be negligible. Also if the values of two or more lifetimes are close together, they may not be separated in the experiment, and effectively the sum of the respective DAS is observed. This is enhanced if the shapes of the respective DAS are similar.

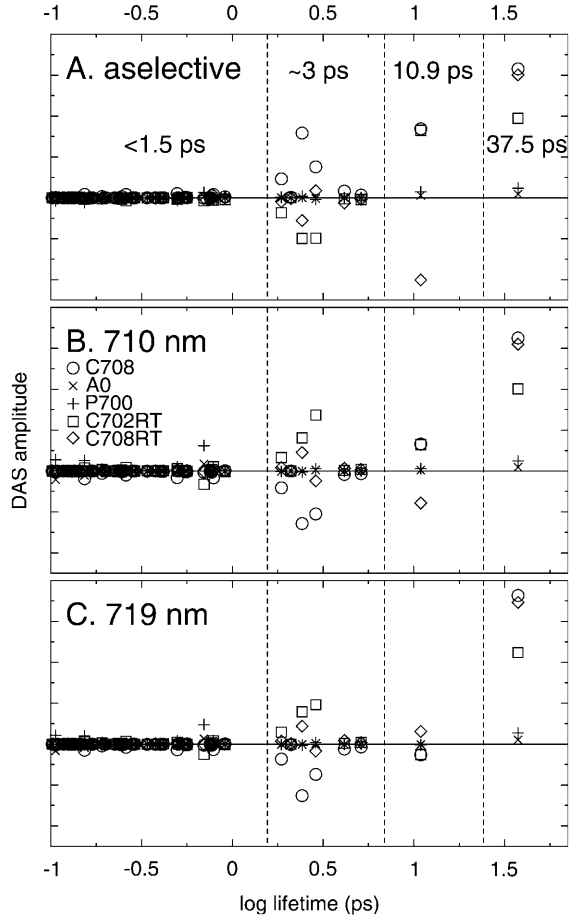

FIGURE 5 Contributions of the different spectral pools to the decay-associated spectra of all 96 lifetimes occurring in the simulation of *Synechococcus elongatus*, for excitation at 400 nm (*A*), 710 nm (*B*), and 719 nm (*C*). Pools: C680 (*circles*), C708/C702RT (*squares*), C719/C708RT (*diamonds*), *P*700 (*plusses*), and A_0 (*crosses*). Note the four distinct dominant lifetimes that occur, i.e., 37.5 ps, 10.9 ps, ~3 ps, and <1.5 ps. The dashed vertical lines mark the lifetime intervals over which the DAS were summed to obtain the DAS in Fig. 6. For details see text.

In Fig. 5 we have plotted the amplitudes of the contribution to the DAS of each of the five pools for each of the 96 lifetimes in the system (note the logarithmic time-base). Clearly only a few lifetimes correspond to DAS with a significant amplitude. Four clusters of lifetimes dominate the dynamics of the system for all excitation conditions: 37.5 ps, 10.9 ps, ~3 ps, and <1.5 ps. The number of lifetimes and their values correspond remarkably well to the experimentally observed lifetimes of 35–38 ps, 8.7–10 ps, 3.4–4.3 ps, and 0.7–1.6 ps. The relative contributions of the various pools to the slowest (37.5 ps) component are the same for each excitation wavelength, consistent with the observation that the shape of the trapping spectrum is independent of the wavelength of excitation. Note that the absolute amplitude of the trapping component does depend slightly on the wavelength of excitation, indicating an excitation-wavelength dependence of the amount of nonequilibrium trapping. The 10.9-ps component in Fig. 5 shows energy transfer between, on the one hand, the bulk and C708/C702RT pools (*circles* and *squares*) and, on the other hand, the C719/C708RT pool (*diamonds*), consistent with the idea that the former pools equilibrate on a shorter timescale. This is confirmed by the components contributing to the ~3-ps lifetime components, which mainly display energy transfer between the bulk (*circles*) and the C708/C702RT pool (*squares*), and does not involve a significant contribution of the C719/C708RT pool (*diamonds*). The <1.5-ps component is composed of the sum of a large number of short lifetime components. This component shows an enhancement of the amplitude of the *P*700 (*crosses*) and C708/C702RT pools (*squares*) for 710/719-nm excitation as compared to aselective excitation.

In Fig. 6 we present the actual dominant DAS resulting from the simulation, which were constructed using the emission-spectra of the various PSI pools as reported in Gobets and van Grondelle (2001) and Gobets et al. (2001). The DAS were summed over the intervals indicated by the dashed vertical lines in Fig. 5, to obtain four effective DAS corresponding to the four lifetimes indicated above. This allows for a direct comparison between the simulated DAS of Fig. 6 and the measured DAS of Fig. 4 (Fig. 6 *a* corresponds to aselective excitation and should be compared to Fig. 4, *a* and *b*). The fastest two downhill energy-transfer components of the simulation have a similar shape, but the ~3-ps contribution (*dashed*) dominates the sub-ps equilibration (*solid*) in amplitude, in accordance with the measurements. The shape and total amplitude of the fast downhill transfer component are quite similar to those observed in the measurements. The experimental data show a distinctly nonconservative 8.7-ps component that accounts for both downhill energy-transfer and nonequilibrium

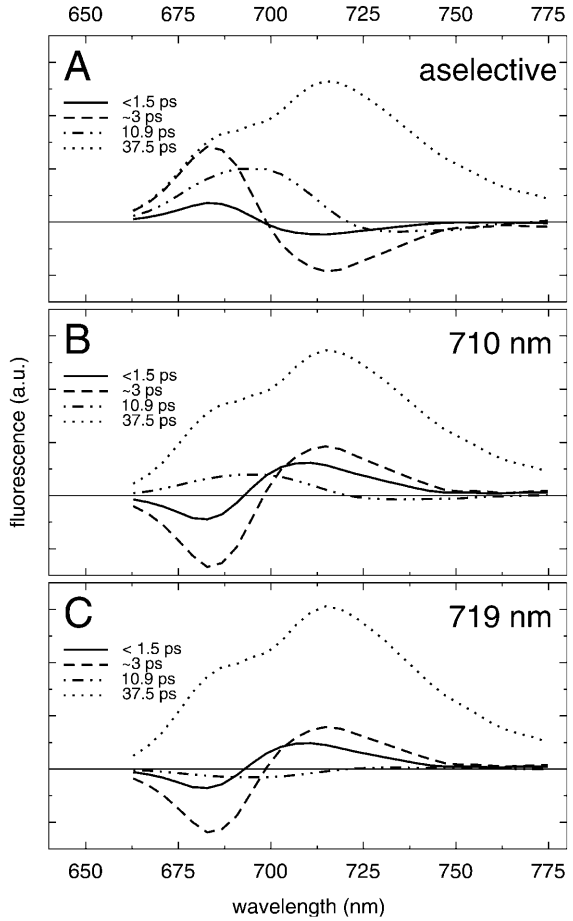

FIGURE 6 Simulated decay-associated spectra of fluorescence decay of trimeric PSI from *Synechococcus elongatus* for excitation at 400 nm (*A*), 710 nm (*B*), and 719 nm (*C*).

trapping. This striking feature is reproduced remarkably well by the simulated 10.9-ps component (*double-dot-dashed*) in Fig. 6 *a*, which is clearly highly nonconservative. The trap spectrum (*dotted*) resembles the measured trap spectrum quite well, although the shoulder representing the bulk antenna chls is somewhat high. This may be the result of employing a spectrally homogeneous bulk antenna. For a heterogeneous bulk antenna the bulk emission would be broader, and therefore the shoulder would be less distinct.

For excitation at 710 nm, the fast equilibration components are both uphill. The sub-ps contribution is considerably larger as compared to aselective excitation conditions, and therefore the mixture of the sub ps and ~3 ps DAS is fitted in the experiment with a faster lifetime as for aselective excitation. The spectral differences between the fastest DAS in the simulation and the experiment occur because we do not include inhomogeneous broadening in the simulation. The excitation pulse in the experiment has a spectral width of ~10 nm and selectively excites an energetic subfraction of the inhomogeneous distributions of the various pools. Energy transfer within the inhomogeneously broadened pools results in the much narrower positive region of the fast energy-transfer DAS and the slightly negative region in the red that are not present in the simulated spectrum. Markedly similar to the experiment, the 10.9-ps DAS shows downhill energy-transfer with the same characteristics as for aselective excitation, albeit with a lower amplitude. As pointed out above, the trapping component has the same shape and approximate amplitude as for the simulation for aselective excitation.

For extremely red excitation at 719 nm, the fast uphill transfer component is similar to that found for 710-nm excitation, i.e., a mixture of a ~3-ps and a sub-ps component. Differences between the experimental and simulated spectrum result from inhomogeneous broadening in a similar way as described above. The amplitude of the 10.9-ps component is negligible in the simulation, consistent with the experiment in which no such slow transfer component could be distinguished at all. The shape of the trapping spectrum is identical to that for the other wavelengths of excitation, but the amplitude is significantly higher, indicating that the amount of nonequilibrium trapping is lower with respect to shorter wavelength excitation.

We would like to emphasize that the simulation lifetimes and the DAS in Fig. 6 resemble the experimental lifetimes and DAS of Fig. 4 remarkably well, especially considering the fact that the simulation did not contain any ''free'' parameters, with the exception of the choice of the red chl sites (which was, in fact, also restricted by only using the most strongly coupled chl*a* dimers/trimer appearing in the structure).

We also attempted to perform the simulations using other assignments of the red chls. This included different permutations of the dimers/trimer indicated by Jordan et al. (2001), the inclusion of the three additional dimers that were introduced above, as well as the assignment by Damjanovic et al. (2002) with the A31/B6/A32/B7 cluster assigned to the C719/C708RT pool. From these simulations it appeared that out of all these aggregates, the trimer is the only suitable candidate for the C719/C708RT pool. The use of any of the dimers (either alone or in combination with another dimer, including the A31/B6/A32/B7 cluster proposed by Damjanovic et al., 2002, and Byrdin et al., 2002) to represent the C719/C708RT pool did not result in a distinct separation of an ~10-ps transfer component from the faster transfer components. It appears that the whole C719/C708RT pool needs to be located in one single cluster in the periphery of the antenna. We therefore propose that the A32/B7 dimer does not constitute part of the C719/C708RT pool, as suggested previously by Jordan et al. (2001), but that instead the trimer consisting of chls B31/B32/B33 is a much better candidate. The assignment of the trimer of chlorophylls (B31/B32/B33) to C719 is further supported by structural and biochemical data for *Synechococcus elongatus* and *Synechocystis* PCC 6803 PSI, based on the observation that *Synechocystis* PCC 6803 PSI lacks a C719 pool. A lumenal loop structure in PsaB which stabilizes the chlorophyll trimer

is shorter in *Synechocystis*, subunit PsaX which interacts with one of the chlorophylls is probably not present in *Synechocystis*, and the axial ligand to B31 (His-B470; Fromme et al., 2001) is not conserved in *Synechocystis* (see also Byrdin et al., 2002, and Sener et al., 2002). According to these observations, the presence of a complete trimer like in *Synechococcus elongatus* PSI seems to be unlikely for *Synechocystis* PCC 6803 PSI (N. Krauss, P. Jordan, and P. Fromme, personal communication).

The assignment of the chls constituting the C708/C702RT pool appears to be less unambiguous: different selections of three out of the total of the six candidate dimers (A32/B7, A38/A39, B37/B38, A12/A14, A10/A18, and B09/B17) generally resulted in an acceptable simulation.

To investigate whether the so-called linker-chls, A40 and B39, perform an important bridging role in the excitation transfer to the RC, we performed the simulation under exactly the same conditions as discussed above, with the only difference being that these linker-chls were removed. The resulting simulation appeared almost identical to the one in which the linker chls were included, with only slightly increased values of the dominant lifetimes and a trapping time which was slowed down by only 2%. Therefore we conclude that the linker chls do not perform a special role in the energy transfer to the RC.

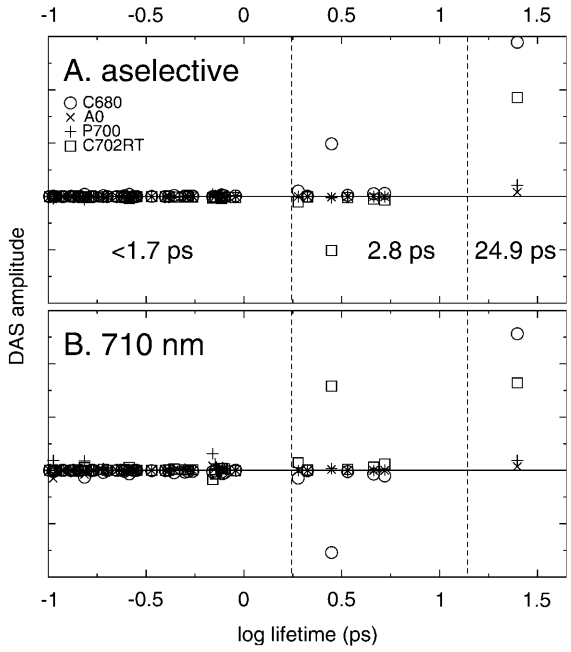

FIGURE 7 Contributions of the different spectral pools to the decay-associated spectra of all 96 lifetimes occurring in the simulation of (trimeric) *Synechocystis* PCC6803, for excitation at 400 nm (*A*) and 710 nm (*B*). Pools: C680 (*circles*), C702RT (*squares*), *P*700 (*plusses*), and A_0 (*crosses*). Note that only three distinct dominant lifetimes occur, i.e., 24.9 ps, 2.8 ps, and <1.7 ps. The dashed vertical lines mark the lifetime intervals over which the DAS were summed to obtain the DAS in Fig. 8. For details see text.

Simulation of the dynamics in trimeric *Synechocystis* PSI

Since a structural model is only available for PSI from *Synechococcus* PSI, we have to assume that the differences with *Synechocystis* PSI are sufficiently small to allow for a simulation based upon the *Synechococcus* structure. We do know that *Synechocystis* PSI, like *Synechococcus* trimeric PSI, contains a pool of C708/C702RT chls and that it lacks the C719/C708RT pool present in this species (Gobets and van Grondelle, 2001). Since the number of C708/C702RT chls in *Synechocystis* trimeric PSI and *Synechococcus* trimeric PSI is about the same, the most straightforward way of simulating the kinetics in *Synechocystis* trimeric PSI is simply to ''remove'' the C719/C708RT trimer, i.e., treat those as ''normal'' antenna chls. *Synechocystis* monomeric PSI contains fewer C708/C702RT chls than the trimers, but since its dynamics is similar, we refrain from a separate simulation of the excitation transfer dynamics in the monomers.

We consider two excitation conditions: aselective and selective at 710 nm (excitation of the chls in the *P*700 and C708/702RT pools with equal probability). This results in the DAS-amplitude versus lifetime plots of Fig. 7, which is the *Synechocystis* PSI trimers' equivalent of Fig. 5. In contrast to the simulation of *Synechococcus* PSI, which exhibits four distinct timescales, only three lifetimes are dominant in *Synechocystis* PSI: 24.9 ps, 2.8 ps, and <1.7 ps, corresponding to the ~23-ps, ~5-ps, and ~1-ps dominant components that are observed in the data. In Fig. 8 we present the DAS resulting from the simulation.

For aselective excitation (Fig. 8 *a*) the slower 2.8-ps downhill transfer component dominates the faster <1.7 ps component, consistent with the measurements. The shape and amplitude of the total energy transfer also correspond reasonably well with the energy-transfer component in Fig. 2, *a–c*, and Fig. 3 *a*. Both the lifetime and the spectrum of the trapping component (*dotted*) match the experimental trapping component remarkably well.

For 710-nm excitation both energy-transfer components are directed uphill. The contribution of the sub-ps component is significantly larger as compared to aselective excitation, consistent with the faster lifetime observed in the experiment. The shape of the trapping spectrum is identical to that found for aselective excitation, but the amplitude is slightly higher, indicating that somewhat less nonequilibrium trapping occurs for selective excitation in the red.

The 2.8-ps lifetime in the simulation of *Synechocystis* PSI is slightly too fast compared to the ~5-ps lifetime that was found in the experiments. The use of other dimers to constitute the C708/C702RT pool did not significantly improve the simulations. Some improvement could be made by using a slightly higher value of $\tau_{ss} = 200$ fs

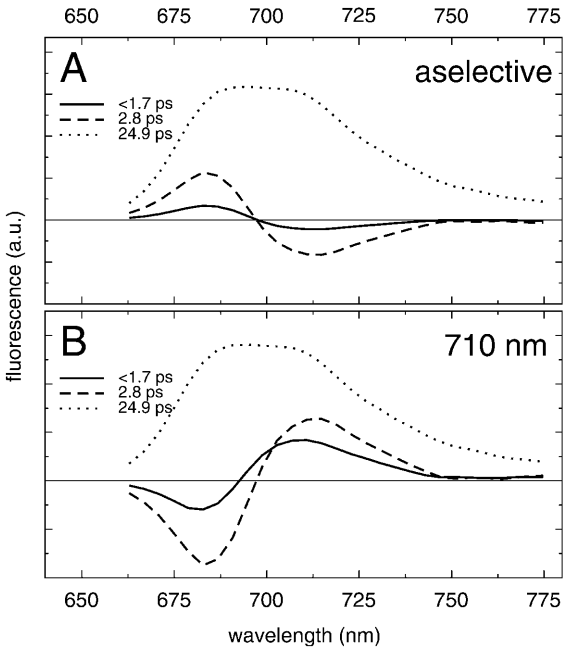

FIGURE 8 Simulated decay-associated spectra of fluorescence decay of trimeric PSI from *Synechocystis* PCC6803 for excitation at 400 nm (*A*) and 710 nm (*B*).

(corresponding to a value of γ of 0.8 ps^{-1} and resulting in an increased value of n from 1.2 to 1.3). This resulted in lifetimes of 24.3 ps, 3.7 ps, and sub-ps, for the spectral composition discussed above.

The ~10-ps component observed for excitation at 702 nm, and to a lesser extent at 710 nm in both monomers and trimers of PSI of *Synechocystis*, could not be reproduced in the simulation. The lifetime and spectrum of this component resemble that of the ~10-ps component in *Synechococcus* PSI, but there it is clearly associated with the presence of the C719/C708RT pool of red chls, which is not present in *Synechocystis* PSI. One could argue that the 10-ps component in *Synechocystis* PSI reflects equilibration with the low-energy fraction of the inhomogeneously broadened C708/C702RT pool (Gobets et al., 1994), which is not accounted for in the simulations. However, this does not explain why the 10-ps component is absent in the dynamics observed upon aselective excitation. The fact that the 10-ps component in *Synechocystis* PSI is large for 702-nm excitation suggests that the process may be linked to the direct excitation of a considerable fraction of *P*700. One might think about charge recombination fluorescence from the $P700^+A_0^-$ state, which is expected to have a lifetime of the order of 10 ps. However, the energy difference between *P*700* and $P700^+A_0^-$ is so large that no significant amount of recombination fluorescence is expected (Brettel and Leibl, 2001). The low light intensities and laser repetition rates used rule out that the 10-ps component is the result of singlet-singlet annihilation or the accumulation of $P700^+$.

In both PSI species the simulations for aselective and selective (red) excitation show a significant difference in the amplitude ratio between the ~3-ps component and the sub-ps component. If one assumes that in the analysis of the experiment one actually fits the mixture of these two components with only one lifetime, one expects the fitted lifetime to be longer for downhill and shorter for uphill energy transfer. Thus the simulations are in accordance with the experimental results. However, the difference in amplitude ratio between the ~3-ps component and the sub-ps component found in the simulations may not be large enough to account for the experimentally observed factor of 3:6 difference in the measured lifetimes. We note that the amplitude of the sub-ps component strongly depends on the initial density of excitations on *P*700. As expressed above, in the experiments with selective red excitation the polarization of detection was perpendicular to the exciting light. We therefore also calculated polarized DAS (not shown) to determine if the large lifetime-difference could be due to depolarization, but we found that the differences between the polarized DAS and the magic angle DAS presented above are small.

CONCLUSIONS

We have shown that the excitation dynamics in PSI from *Synechocystis* and *Synechococcus* differ significantly. Furthermore, for each species the dynamics depends strongly on the initially excited distribution of pigments.

For aselective excitation the fastest downhill energy-transfer occurred between the bulk and the C702RT pool with a lifetime of 3.4–5.5 ps. For selective excitation of the red chl pools, uphill transfer between the same two pools occurs much faster, in ~1 ps. Such a difference between the uphill and downhill energy-transfer lifetimes in PSI has not been reported before. By interpreting both lifetimes as a mixture of lifetimes this compelling difference could, to a certain extent, be explained in a structure-based simulation, which demonstrated that the amplitude ratio between the faster and slower contributions shifts toward the faster lifetimes upon red chl excitation, especially if some direct excitation of *P*700 is taken into account.

In *Synechococcus* PSI an additional, significantly slower equilibration process occurs in ~10 ps, which is mainly associated with energy transfer between the bulk and C702RT pool on the one hand, and the C719/C708RT pool on the other hand, and which also accounts for a significant amount of nonequilibrium trapping. For all wavelengths of excitation both the lifetime and the nonconservative spectrum of this component were reproduced remarkably well in the simulation, provided that the chls B31, B32, and B33 constituting the trimer reported by Jordan et al. (2001) were used for the C719/C708RT pool. The choice of this trimer was corroborated by structural and biochemical data for *Synechococcus* and *Synechocystis* PSI (N. Krauss,

P. Jordan, and P. Fromme, personal communication). The assignment of the chls constituting the C702RT pool was less crucial; combinations of the three dimers reported by Jordan and co-workers (i.e., A32/B7, A38/A39, and B37/B38; Jordan et al., 2001) and three more dimers proposed in this contribution (A12/A14, A10/A18, and B09/B17) all resulted in more or less reasonable lifetimes and spectra.

Each of the species exhibits its own characteristic trap spectrum, the shape of which is independent of the wavelength of excitation. This trap spectrum decays in ~23 ps in both monomeric and trimeric *Synechocystis* PSI and in ~35 ps in trimeric *Synechococcus* PSI. These lifetimes and spectra were reproduced very well in the simulation.

The presence of a significant ~10-ps component, upon 702-nm excitation in *Synechocystis* PSI, exhibiting an all-positive spectrum, could not be reproduced in the simulation. Furthermore, the simulation revealed that the so-called linker chls do not perform a special role in the process of energy transfer to the RC.

In the simulations we have used only one pool of red chls (C708/C702RT) for the modeling of *Synechocystis* PSI and two pools (C708/C702RT) and (C719/C708RT) for *Synechococcus* PSI. As mentioned in the introduction, low temperature hole-burning experiments suggest the presence of an additional pool with an absorption maximum of 714–715 nm in both species. In our room-temperature data such an additional pool was not resolved. The spectral separation of the red pools is much smaller at room temperature than at 4 K, which might ''hide'' an additional pool. Since we propose three distinctly different dimers to be responsible for the C708 pool, it could be possible that some heterogeneity occurs in this pool. If the spectral differences are, however, not too large, the kinetics will remain within the same distributions of lifetimes (Figs. 5 and 7), and the heterogeneity will not be resolved experimentally.

We thank N. Krauss, P. Jordan, and P. Fromme for sharing unpublished work. We thank Matthias Rögner, Jochen Kruip, and Eberhard Schlodder for providing the PSI preparations investigated in this work.

This research was supported by the Netherlands Organization for Scientific Research via the Dutch Foundation of Earth and Life Sciences (ALW). The streak camera and amplified Ti:Sapph laser system were funded by investment grants of ALW.

REFERENCES

Brettel, K., and W. Leibl. 2001. Electron transfer in Photosystem I. *Biochim. Biophys. Acta*. 1507:100–114.

Byrdin, M., I. Rimke, E. Schlodder, D. Stehlik, and T. A. Roelofs. 2000. Decay kinetics and quantum yields of fluorescence in Photosystem I from *Synechococcus elongatus* with *P*700 in the reduced and oxidized state: are the kinetics of excited state decay trap-limited or transfer-limited? *Biophys. J*. 79:992–1007.

Byrdin, M., P. Jordan, N. Krauss, P. Fromme, D. Stehlik, and E. Schlodder. 2002. Light harvesting in Photosystem I: modeling based on the 2.5-Ångstrom structure of Photosystem I from *Synechococcus elongatus*. *Biophys. J*. 83:433–457.

Damjanovic, A., H. M. Vaswani, P. Fromme, and G. R. Fleming. 2002. Chlorophyll excitations in Photosystem I of *Synechococcus elongatus*. *J. Phys. Chem. B*. 106:10251–10262.

Du, M., X. Xie, Y. Jia, L. Mets, and G. R. Fleming. 1993. Direct observation of ultrafast energy transfer in PS I core antenna. *Chem. Phys. Lett*. 201:535–542.

Förster, T. 1965. Modern Quantum Chemistry. O. Sinanoglu, editor. Academic Press, New York. 93–137.

Fromme, P., and H. T. Witt. 1998. Improved isolation and crystallization of Photosystem I for structural analysis. *Biochim. Biophys. Acta*. 1365:175–184.

Fromme, P., P. Jordan, and N. Krauss. 2001. Structure of Photosystem I. *Biochim. Biophys. Acta*. 1507:5–31.

Gobets, B., I. H. M. van Stokkum, F. van Mourik, M. Rögner, J. Kruip, J. P. Dekker, and R. van Grondelle. 1998a. Time-resolved fluorescence measurements of Photosystem I from *Synechocystis* PCC 6803. *In* Photosynthesis: Mechanisms and Effects. G. Garab, editor. Kluwer Academic Publishers, Dordrecht, The Netherlands. 571–574.

Gobets, B., J. P. Dekker, and R. van Grondelle. 1998b. Transfer-to-the-trap limited model of energy transfer in Photosystem I. *In* Photosynthesis: Mechanisms and Effects. G. Garab, editor. Kluwer Academic Publishers, Dordrecht, The Netherlands. 503–508.

Gobets, B., H. van Amerongen, R. Monshouwer, Y. Kruip, M. Rögner, R. van Grondelle, and J. P. Dekker. 1994. Polarized site-selected fluorescence spectroscopy of isolated Photosystem I particles. *Biochim. Biophys. Acta*. 1188:75–85.

Gobets, B., I. H. M. van Stokkum, M. Rögner, J. Kruip, E. Schlodder, N. V. Karapetyan, J. P. Dekker, and R. van Grondelle. 2001. Time-resolved fluorescence emission measurements of Photosystem I particles of various cyanobacteria: a unified compartmental model. *Biophys. J*. 81:407–424.

Gobets, B., and R. van Grondelle. 2001. Energy transfer and trapping in Photosystem I. *Biochim. Biophys. Acta*. 1507:80–99.

Hastings, G., L. J. Reed, S. Lin, and R. E. Blankenship. 1995. Excited state dynamics in Photosystem I: effects of detergent and excitation wavelength. *Biophys. J*. 69:2044–2055.

Hayes, J. M., S. Matsuzaki, M. Rätsep, and G. J. Small. 2000. Red chlorophyll-*a* antenna states of Photosystem I of the cyanobacterium *Synechocystis* sp. PCC 6803. *J. Phys. Chem. B*. 104:5625–5633.

Holzwarth, A. R., G. Schatz, H. Brock, and E. Bittersmann. 1993. Energy transfer and charge separation kinetics in Photosystem I. Part 1: picosecond transient absorption and fluorescence study of cyanobacterial Photosystem I particles. *Biophys. J*. 64:1813–1826.

Ihalainen, J. A., M. Rätsep, P. E. Jensen, H. V. Scheller, R. Croce, R. Bassi, J. E. I. Korppi-Tommola, and A. Freiberg. 2003. Red spectral forms of chlorophylls in green plant PSI—a site-selective and high-pressure spectroscopy study. *J. Phys. Chem. B*. On the web.

Jordan, P., P. Fromme, H. T. Witt, O. Klukas, W. Saenger, and N. Krauss. 2001. Three-dimensional structure of cyanobacterial Photosystem I at 2.5 Ångstrom resolution. *Nature*. 411:909–917.

Karapetyan, N. V., A. R. Holzwarth, and M. Rögner. 1999. The Photosystem I trimer of cyanobacteria: molecular organization, excitation dynamics and physiological significance. *FEBS Lett*. 460:395–400.

Kennis, J. T. M., B. Gobets, I. H. M. van Stokkum, J. P. Dekker, R. van Grondelle, and G. R. Fleming. 2001. Light harvesting by chlorophylls and carotenoids in the Photosystem I complex of *Synechococcus elongatus*: a fluorescence upconversion study. *J. Phys. Chem. B*. 105:4485–4494.

Kleima, F. J., E. Hofmann, B. Gobets, I. H. M. van Stokkum, R. van Grondelle, K. Diederichs, and H. van Amerongen. 2000. Förster excitation energy transfer in peridinin-chlorophyll-*a*-protein. *Biophys. J*. 78:344–353.

Kumazaki, S., H. Kandori, H. Petek, K. Yoshihara, and I. Ikegami. 1994. Primary photochemical processes in *P*700-enriched Photosystem-I

particles—trap-limited excitation decay and primary charge separation. *J. Phys. Chem.* 98:10335–10342.

Krauss, N., W.-D. Schubert, O. Klukas, P. Fromme, H. T. Witt, and W. Saenger. 1996. Photosystem I at 4 Å resolution represents the first structural model of a joint photosynthetic reaction centre and core antenna system. *Nat. Struct. Biol.* 3:965–973.

Kruip, J., E. J. Boekema, D. Bald, A. F. Boonstra, and M. Rögner. 1993. Isolation and structural characterization of monomeric and trimeric Photosystem-I complexes ($P700{\cdot}F_a/F_b$ and $P700{\cdot}F_x$) from the cyanobacterium *Synechocystis* PCC-6803. *J. Biol. Chem.* 268:23353–23360.

Kruip, J., D. Bald, E. Boekema, and M. Rögner. 1994. Evidence for the existence of trimeric and monomeric Photosystem I complexes in thylakoid membranes from cyanobacteria. *Photosynth. Res.* 40:279–286.

Lichtenthaler, H. K. 1987. Chlorophylls and carotenoids: pigments of photosynthetic membranes. *Methods Enzymol.* 148:350–382.

Melkozernov, A. N., S. Lin, and R. E. Blankenship. 2000. Excitation dynamics and heterogeneity of energy equilibration in the core antenna of Photosystem I from the cyanobacterium *Synechocystis* sp. PCC 6803. *Biochemistry.* 39:1489–1498.

Mukerji, I., and K. Sauer. 1990. A spectroscopic study of a Photosystem I antenna complex. *In* Current Research in Photosynthesis. M. Baltscheffsky, editor. Kluwer Academic Publishers, Dordrecht, The Netherlands. 321–324.

Pålsson, L.-O., J. P. Dekker, E. Schlodder, R. Monshouwer, and R. van Grondelle. 1996. Polarized site-selective fluorescence spectroscopy of the long-wavelength emitting chlorophylls in isolated Photosystem I particles of *Synechococcus elongatus*. *Photosynth. Res.* 48:239–246.

Pålsson, L.-O., C. Flemming, B. Gobets, R. van Grondelle, J. P. Dekker, and E. Schlodder. 1998. Energy transfer and charge separation in Photosystem I: *P*700 oxidation upon selective excitation of the long-wavelength chlorophylls of *Synechococcus elongatus*. *Biophys. J.* 74:2611–2622.

Rätsep, M., T. W. Johnson, P. R. Chitnis, and G. J. Small. 2000. The red-absorbing chlorophyll-*a* antenna states of Photosystem I: a hole-burning study of *Synechocystis* sp PCC 6803 and its mutants. *J. Phys. Chem. B.* 104:836–847.

Rivadossi, A., G. Zucchelli, F. M. Garlaschi, and R. C. Jennings. 1999. The importance of PSI chlorophyll red forms in light-harvesting by leaves. *Photosynth. Res.* 60:209–215.

Savikhin, S., W. Xu, V. Soukoulis, P. R. Chitnis, and W. S. Struve. 1999. Ultrafast primary processes in Photosystem I of the cyanobacterium *Synechocystis* sp. PCC 6803. *Biophys. J.* 76:3278–3288.

Savikhin, S., W. Xu, P. R. Chitnis, and W. S. Struve. 2000. Ultrafast primary processes in PS I from *Synechocystis* sp. PCC 6803: roles of *P*700 and A_0. *Biophys. J.* 79:1573–1586.

Scheller, H. V., H. Naver, and B. L. Moller. 1997. Molecular aspects of Photosystem I. *Physiol. Plant.* 100:842–851.

Scheller, H. V., P. E. Jensen, A. Haldrup, C. Lunde, and J. Knoetzel. 2001. Role of subunits in eukaryotic Photosystem I. *Biochim. Biophys. Acta.* 1507:41–60.

Schubert, W.-D., O. Klukas, N. Krauss, W. Saenger, P. Fromme, and H. T. Witt. 1997. Photosystem I of *Synechococcus elongatus* at 4 Å resolution: comprehensive structure analysis. *J. Mol. Biol.* 272:741–769.

Schwabe, T. M. E., E. J. Boekema, S. Berry, P. R. Chitnis, E. Pistorius, and J. Kruip. 2001. Dynamics of Photosystem I: Ca^{2+}-based oligomerization and response to iron deficiency by induction of a new antenna built by IsiA. *In* Proceedings of the 12th International Congress on Photosynthesis. B. Osmond, editor. CSIRO Publishing, Brisbane, Australia. S6:003.

Sener, M. K., D. Y. Lu, T. Ritz, S. Park, P. Fromme, and K. Schulten. 2002. Robustness and optimality of light harvesting in cyanobacterial photosystem I. *J. Phys. Chem. B.* 106:7948–7960.

Trissl, H.-W., and C. Wilhelm. 1993. Why do thylakoid membranes from higher-plants form grana stacks? *Trends Biochem. Sci.* 18:415–419.

Turconi, S., J. Kruip, G. Schweitzer, M. Rögner, and A. R. Holzwarth. 1996. A comparative fluorescence kinetics study of Photosystem I monomers and trimers from *Synechocystis* PCC 6803. *Photosynth. Res.* 49:263–268.

Van Amerongen, H., L. Valkunas, and R. van Grondelle. 2000. Photosynthetic Excitons. World Scientific, London, UK. 347–352.

Van der Lee, J., D. Bald, S. L. S. Kwa, R. van Grondelle, M. Rögner, and J. P. Dekker. 1993. Steady-state polarized-light spectroscopy of isolated Photosystem-I complexes. *Photosynth. Res.* 35:311–321.

Van Grondelle, R., and V. Sundström. 1988. Excitation energy transfer in photosynthesis. *In* Photosynthetic Light-Harvesting Systems. H. Scheer and S. Schneider, editors. De Gruyter, Berlin, Germany. 403–438.

Van Grondelle, R., H. Bergström, V. Sundström, and R. J. van Dorssen. M. Vos, and C.N. Hunter. 1988. Excitation energy transfer in the light-harvesting antenna of photosynthetic purple bacteria: the role of the long-wavelength absorbing pigment B896. *In* Photosynthetic Light-Harvesting Systems. H. Scheer and S. Schneider, editors. De Gruyter, Berlin, Germany. 519–530.

Van Grondelle, R., J. P. Dekker, T. Gillbro, and V. Sundström. 1994. Energy transfer and trapping in photosynthesis. *Biochim. Biophys. Acta.* 1187:1–65.

Werst, M., Y. W. Jia, L. Mets, and G. R. Fleming. 1992. Energy-transfer and trapping in the Photosystem I core antenna—a temperature study. *Biophys. J.* 61:868–878.

Zazubovich, V., S. Matsuzaki, T. W. Johnson, J. M. Hayes, P. R. Chitnis, and G. J. Small. 2002. Red antenna states of Photosystem I from cyanobacterium *Synechococcus elongatus*: a spectral hole-burning study. *Chem. Phys.* 275:47–59.